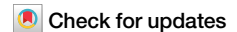
A Nature Portfolio journal



https://doi.org/10.1038/s42005-025-02239-2

Manipulating wetting and pore filling by wall transparency



Svyatoslav Kondrat ^{1,2,3,4} ⊠, Lothar Schimmele^{3,4}, Alberto Giacomello ⁵, Mykola Tasinkevych ^{6,7} & S. Dietrich⁴

Atomically thin walls become increasingly prevalent in modern technologies. Exhibiting a unique property—transparency to interparticle interactions—such walls influence processes as diverse as capacitive energy storage, electron transfer, and wetting. However, the impact of wall transparency on wetting and capillary phenomena remains poorly understood. Herein, we employ classical density functional theory to explore how van der Waals interactions across thin solid walls affect capillarity and substrate wetting. Our findings demonstrate that a fluid-filled, sidewise-open channel beneath a thin wall can drastically enhance the lyophobicity of the wall (hydrophobicity if fluid is water), up to the point of effectively transforming lyophilic surfaces into lyophobic ones. Conversely, a fluid covering a thin wall can convert capillary condensation to drying and induce unusual capillary phases within the channel. These findings highlight the potential of wall transparency as a tool for manipulating channel filling and wetting behaviors, emphasizing its significance for interfacial phenomena and fluid adsorption in porous materials.

Wetting and capillary phenomena¹ play a pivotal role in numerous physical processes, ranging from water transport in plants^{2,3} and joint tribology^{4,5} to superhydrophobicity^{6–8} and microfluidics⁹. Despite extensive theoretical and experimental investigations^{10–12}, most studies have focused on systems with sufficiently thick pore walls so that the interactions among fluid particles from different, wall-separated compartments of the same system can be neglected. However, many technologically important materials, such as metal-organic frameworks (MOFs)^{13,14}, carbon-based microporous electrodes^{15,16}, and particularly low-dimensional materials like graphene¹⁷, carbon nanotubes (CNTs)¹⁸, and MXenes¹⁹, inherently possess atomically thin solid walls. Such walls are often transparent to van der Waals and other interactions, rendering the behavior of fluid particles on opposite sides of the walls to be interdependent.

This cross-wall communication gives rise to feedback mechanisms underpinning nontrivial qualitative effects, emerging as important factors in diverse processes^{20–26}, from charging microporous electrodes^{20,21} to electron transfer in metal ion reduction²⁶. In the context of wetting, Rafiee et al. reported that graphene coating, even up to six layers thick, does not significantly alter the contact angle of water at surfaces for which the wetting behavior is determined by van der Waals interactions²². Most recently, wall transparency has been demonstrated to significantly influence nanoscale

fluid transport, as exemplified by the transparency-induced slowdown of water flow through CNT membranes²⁴ and the phenomenon of "flow tunneling," where two liquids separated by an atomically thin wall exchange momentum²⁵. Despite these advancements, the impact of wall transparency on wetting, pore filling, and capillary condensation remains poorly understood.

Herein, we use classical density functional theory²⁷⁻²⁹ (DFT) to investigate the transparency-driven *interdependence* between channel filling and the contact angle at a thin wall, i.e., we study how a fluid covering an atomically thin wall influences the capillary behavior of an underlying channel and, conversely, how capillary filling of the channel affects the wetting properties of the thin wall (Fig. 1a). Our analysis reveals *three* stable and metastable branches of the contact angle, each associated with a distinct configuration of the capillary fluid. Moreover, we find that wall transparency can increase the contact angle by as much as 60°, effectively transforming lyophilic materials into (super)lyophobic ones. Remarkably, we identify a stable droplet-induced capillary phase featuring a liquid-vapor interface within the channel and show that a vapor phase covering a thin wall can induce capillary drying in channels composed of lyophilic walls—channels that would otherwise remain filled with liquid.

¹Institute of Physical Chemistry, Polish Academy of Sciences, Warsaw, Poland. ²Institute for Computational Physics, University of Stuttgart, Stuttgart, Germany. ³Max Planck Institute for Intelligent Systems, Stuttgart, Germany. ⁴Ivth Institute for Theoretical Physics, University of Stuttgart, Stuttgart, Germany. ⁵Dipartimento di Ingegneria Meccanica e Aerospaziale, Sapienza Università di Roma, Rome, Italy. ⁶SOFT Group, School of Science and Technology, Nottingham Trent University, Nottingham, UK. ⁷International Institute for Sustainability with Knotted Chiral Meta Matter (WPI-SKCM2), Hiroshima University, Hiroshima, Japan.

e-mail: svyatoslav.kondrat@gmail.com; skondrat@ichf.edu.pl

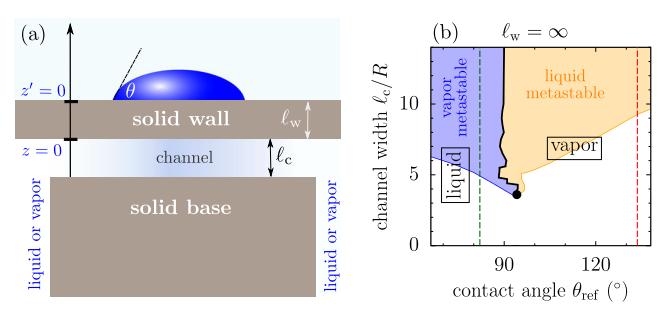


Fig. 1 | Model and channel filling. a Schematic drawing of a thin solid wall of thickness ℓ_w and a channel of width ℓ_c formed by the wall and a thick solid base of the same material as the wall. The channel is connected to a reservoir filled with a fluid at bulk liquid-vapor coexistence. We investigate how ℓ_w affects channel filling, depending on which fluid phase homogeneously covers the upper wall (not shown) and how the wetting properties of the upper wall, expressed in terms of its contact angle θ , change depending on channel filling. b Phase diagram of channel filling for thick walls ($\ell_w = \infty$) in the plane spanned by ℓ_c and the reference contact angle $\theta_{\rm ref}$ between the liquid and solid. The full black line denotes first-order phase transitions between capillary liquid and vapor phases. The black filled circle indicates the critical point. The blue and orange shaded areas show the regions of metastability of the liquid and vapor phases; the thin blue and orange lines show the corresponding spinodals. The vertical dashed lines indicate the values of $\theta_{\rm ref}$ used for Figs. 2 and 3. All values of the model parameters are provided in Supplementary Table S1.

Results

We consider a slit-shaped channel of width ℓ_c formed by a rigid thin solid wall of thickness $\ell_{\rm w}$ (extremely thin walls may experience elastic deformations, giving rise to modulations of the channel width beneath droplets;transparency effects studied in this system will persist in the presence of elastic deformations, but might be undulated) and a thick solid base of the same material as the thin wall (Fig. 1a). The channel is filled with a fluid and is connected to an external reservoir maintained at constant temperature and pressure (or chemical potential, in a grand-canonical ensemble) corresponding to liquid-vapor coexistence. The thin upper wall is covered at the outside with the same type of fluid, which can be in the liquid or the vapor state. In order to isolate generic physical effects from the chemical complexity of fluid molecules and the structural details of solid walls, we modeled the fluid using a truncated Lennard-Jones potential. This widely used model represents a simple yet generic system, capable of exhibiting liquid-gas coexistence. For the solid, we considered a material composed of particles of radius R_s significantly smaller than the radius R of the fluid particles (specifically, $R_s = 0.2R$). This choice enables us to investigate different fluid-wall combinations, including ultra-thin walls. If we take water as the fluid ($R \approx 0.28$ nm), the thickness of a graphene layer ($\ell_w \approx 0.3$ nm) corresponds to a wall comprising about 2.6 solid particles in our model. One-layer walls of our model can be realized by using graphene and colloidal suspensions³⁰ or fluids composed of larger molecules, e.g., perfluoromethylcyclohexane (C₇F₁4), a popular nonpolar, volatile fluid³

We determined the contact angle of a liquid droplet residing on the top of a wall using the macroscopic Young equation

$$\theta = \arccos((\gamma_{vs} - \gamma_{ls})/\gamma_{vl}), \tag{1}$$

where y_{vl} is the vapor-liquid surface tension, while y_{vs} and y_{ls} denote the vapor-solid and the liquid-solid surface tension, respectively. We computed y_{vb} y_{vs} , and y_{ls} numerically for various configurations using classical density functional theory (DFT), in which the equilibrium density profiles are obtained by minimizing the grand thermodynamic potential^{27–29}. In our DFT calculations, the repulsive steric interactions were captured by using a robust fundamental measure theory (FMT)^{32–34}, while the attractive van der Waals interactions were treated at the level of mean-field theory (MFT) (see Methods and Supplementary Note 2 for details). We note that MFT neglects thermal fluctuations. However, since the phenomena discussed here are

primarily governed by the long-ranged nature of van der Waals interactions, we expect that our findings remain valid even if such fluctuations are included. Nonetheless, incorporating fluctuations explicitly within DFT could be an interesting extension of this work. Such promising approaches include perturbative schemes³⁵ and machine-learning-assisted DFT³⁶.

Capillary transitions in channels with thick walls

We first examined the filling of channels composed of macroscopically thick walls. We varied systematically the channel width ℓ_c and the strength of the fluid-wall interaction. The latter controls the reference contact angle θ_{ref} between the liquid drop and a thick solid slab, which serves as an experimentally accessible characteristic of the fluid-solid system.

Figure 1b presents a capillary phase diagram, which shows a line of first-order (discontinuous) transitions separating the regions where the capillary liquid and the capillary vapor phases are stable. This line terminates at a critical point $(\theta^c_{\rm ref}, \ell^c_c)$, implying that the fluid density varies continuously with $\theta_{\rm ref}$ for $\ell_c < \ell^c_c$.

For $\ell_c \gtrsim 10R$, the capillary vapor and liquid coexist at $\theta_{\rm ref} \approx 90^\circ$, in agreement with the predictions of the macroscopic Kelvin-Laplace equation^{37,38}. For $\ell_c \lesssim 10R$, the line of first-order transitions exhibits step-like oscillations close to the critical point (we note that this step-like coexistence curve may change if we account for fluctuations). This behavior stems from fluid layering within the channel in the capillary liquid phase. Upon widening the channel from $\ell_c = 4R$ (two layers) to $\ell_c = 5R$, the vapor phase becomes more stable than the liquid phase due to the incommensurate number of layers in the channel. However, further widening the channel to $\ell_c = 6R$ (three layers) enhances the stability of the liquid phase because the channel acquires an additional full layer of the particles forming the fluid. Consequently, for moderately lyophilic walls, in a small interval around $\theta_{\rm ref} \approx 90^\circ$, the system undergoes a cascade of reentrant transitions upon varying the channel width (Supplementary Fig. S2).

Interdependence of wetting and pore filling for thin walls

For a wall thinner than the range of the fluid-fluid interaction, a fluid molecule can interact with fluid particles on both sides of the wall. Consequently, the surface tensions γ_{vs} and γ_{ls} in Eq. (1), and hence the contact angle θ_{co} depend on whether the channel is filled with vapor (α = v) or liquid (α = l). Conversely, the channel filling depends on whether the thin wall is covered by liquid or vapor.

In order to relate the contact angle and channel filling, we note that the stability of the capillary liquid phase over the capillary vapor phase is determined by the difference $\Delta\Omega$ of their respective grand potentials. At vapor-liquid coexistence and for wide channels, $\Delta\Omega$ depends solely on the corresponding surface tensions. Using the Young equation, Eq. (1), one can show that for the upper thin wall covered with a fluid in state α , the capillary vapor phase is stable if (Supplementary Note 3)

$$\Delta\omega_{\alpha} \equiv \cos\theta_{\alpha}(\ell_{\rm w}) + \cos\theta_{\rm bot} < 0; \tag{2}$$

conversely, the capillary liquid phase is stable if $\Delta\omega_{\alpha} > 0$. Here, $\theta_{\alpha}(\ell_{w})$ and θ_{bot} are the contact angles of the thin upper wall if the other side of the wall is covered by phase α and of the bottom wall, respectively ($\theta_{bot} = \theta_{ref}$ for the upper and bottom walls made of the same material). Note that θ_{α} is independent of ℓ_{c} because the above analysis assumes wide channels. However, in the analysis below, we also consider narrow channels, for which θ_{α} varies with ℓ_{c} .

Thin lyophobic walls

We consider now a specific example of lyophobic solids with $\theta_{\rm ref} \approx 133$. 6°. Figure 2a, b depict density profiles for liquid and vapor covering the thin wall, respectively, and for several channel widths ℓ_c . These figures illustrate the *duality* of wall transparency. On one hand, the fluid-filled channel affects substantially the structure of the liquid layer adsorbed at the upper wall. In particular, the capillary vapor induces a depletion layer ($\ell_c/R = 7$ in Fig. 2a) while the capillary liquid leads to an enhanced density at the upper wall ($\ell_c/R = 10$ and $\ell_c/R = 15$ in Fig. 2a). On the other hand, the fluid covering the

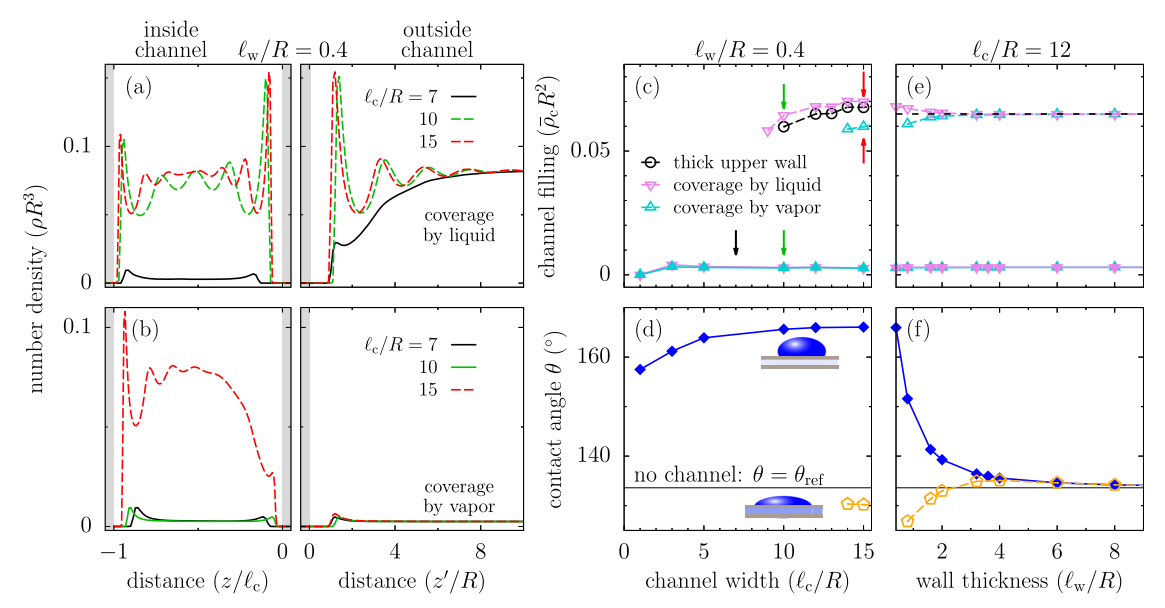


Fig. 2 | Lyophobic walls. Number density profiles for three values of the channel width ℓ_c with a liquid and b vapor covering the outside of the upper wall of the channel (Fig. 1a). Here the left plots show the densities inside the channel with the position expressed in terms of ℓ_c . The right plots show the densities outside the channel above its upper wall, with the distance from the wall measured in units of the radius R of the fluid particles. The fluid density vanishes in the gray depletion zone. Filling of the channel by liquid is metastable in all cases. The wall thickness is $\ell_w/R = 0.4$. c Average fluid number density $\bar{\rho}_c$ inside the channel as a function of the channel width ℓ_c for a thick wall ($\ell_w \to \infty$) and for $\ell_w/R = 0.4$ in the case of coverage by liquid or vapor. In all plots and throughout the paper, the filled symbols and solid

lines (open symbols and dashed lines) correspond to stable (metastable) configurations. The lines associated with metastable configurations end once they cease to exist. The various colored arrows indicate the values of ℓ_c/R and $\bar{\eta}_c$ corresponding to the profiles shown in (\mathbf{a},\mathbf{b}) with the same color code. \mathbf{d} Contact angle θ for channels filled with liquid and vapor, as illustrated by the droplet cartoons (for visualization purposes only). The contact angles were computed from the surface tensions of the corresponding configurations according to Eq. (1). The horizontal line indicates the reference contact angle $\theta_{\rm ref} \approx 133$. 6° (no channel; see the dashed red vertical line in Fig. 1b). \mathbf{e} , \mathbf{f} The same quantity as in (\mathbf{c},\mathbf{d}) but as functions of wall thickness $\ell_{\rm w}$ for a channel of width $\ell_c/R=12$.

upper wall influences the structure of the fluid inside the channel. Specifically, the liquid coverage induces a capillary liquid phase ($\ell_c/R=10$ in Fig. 2a, b; see also below), while the vapor coverage leads to a drastic asymmetry of the density profile of the capillary liquid, resembling a liquid-vapor interface³⁹ ($\ell_c/R=15$ in Fig. 2b). The asymmetry emerges because the vapor phase above the thin wall acts as an ℓ_w and ℓ_c -dependent external field, promoting the drying-like condition at this wall.

In Fig. 2c, we show the average fluid number density inside the channel, $\bar{\rho}_c = (1/\ell_c) \times \int_0^{\ell_c} \rho(z) dz$, as a function of ℓ_c . For thick walls, the capillary vapor remains stable for all channel widths ℓ_\odot while a metastable capillary liquid appears for $\ell_c/R \gtrsim 10$ (see the filled and open black circles in Fig. 2c, respectively, as well as the red dashed line in Fig. 1b). Thin walls retain the stability of the capillary vapor but shift the capillary liquid spinodal to larger or smaller values of ℓ_\odot depending on whether the upper wall is covered by vapor or liquid, respectively.

In order to show the effect of channel filling on the wetting properties of the upper (transparent) wall, in Fig. 2d we plot the contact angle θ as a function of ℓ_c . Two distinct situations arise depending on whether the fluid density inside the channel is liquid-like or vapor-like. Correspondingly, we obtained θ by using γ_{vs} and γ_{ls} of the upper wall, both computed either for vapor-filled or liquid-filled channels. In the capillary liquid case, which is metastable and appears only for $\ell_c/R \gtrsim 14$, the contact angle θ is slightly lower than θ_{ref} . Thus, as one may anticipate, filling the channel with liquid decreases the overall surface lyophobicity because of stronger attractive interactions through the transparent wall. Conversely, the vapor-filled channel drastically enhances lyophobicity due to weaker interactions as compared to the thick-wall and the liquid-filled channels, yielding contact angles of about 30° higher than θ_{ref} . We emphasize that the capillary vapor phase is stable irrespective of whether the upper wall is covered by liquid or vapor. This is consistent with the stability condition, Eq. (2), which gives $\Delta \omega_{\rm v} \approx -1.3 < 0$ and $\Delta \omega_{\rm l} \approx -1.6 < 0$.

Figure 2e, f show pore filling and contact angles, respectively, as functions of the wall thickness ℓ_{wz} demonstrating that the observed effects

persist as ℓ_w increases, albeit with reduced strength. The shift of the spinodal of the confined liquid becomes smaller, whereas the capillary vapor provides a noticeable enhancement in lyophobicity in terms of the contact angle even for $\ell_w \approx 2R$, which is slightly smaller than two graphene layers ($R \approx 0.67$ nm) in the case of water ($R \approx 0.28$ nm).

Moderately lyophilic thin walls

Condition (2) implies that the wall coverage can have a more substantial effect on the stability of capillary phases if θ_{ref} is closer to 90°. In order to demonstrate this, we consider moderately lyophilic walls characterized by $\theta_{\rm ref} \approx 82^{\circ}$. For thick walls, the capillary liquid remains stable for all channel widths investigated, with metastable capillary vapor emerging for $\ell_c/R \gtrsim 4.5$ (green line in Fig. 1b and Supplementary Fig. S3). Wall transparency significantly changes this behavior and renders channel filling markedly dependent on the upper wall coverage. Counterintuitively, liquid coverage extends the region of metastability of the capillary vapor; otherwise, however, it shows moderate changes in the filling as compared with the case of thick walls (Fig. 3a). The vapor coverage, instead, interchanges the stability of the capillary liquid (stable for thick walls) with the capillary vapor (metastable for thick walls) and induces appreciable changes in the liquid density (Fig. 3b). Such drastic changes arise due to the significant reduction in interactions between fluid particles inside the channel and particles outside the channel if the upper wall is in contact with a rarefied phase, as compared to the presence of condensed phases (solid or liquid-covered wall).

The observed behavior has implications for the contact angle of the upper wall. Figure 3c shows that there are three scenarios: (i) the channel is filled with vapor, (ii) it contains liquid, and (iii) a liquid-vapor interface forms within the channel. Case (i) resembles lyophobic walls in that the vapor filling notably increases the contact angle (even up to 60°, from 80° to 140°, see the blue diamonds in Fig. 3c). However, unlike lyophobic walls, this configuration is metastable. Surprisingly, the liquid filling of the channel also *increases* the contact angle of the upper wall (orange pentagons in Fig. 3c). This phenomenon arises from the intricate interplay between wall-fluid and

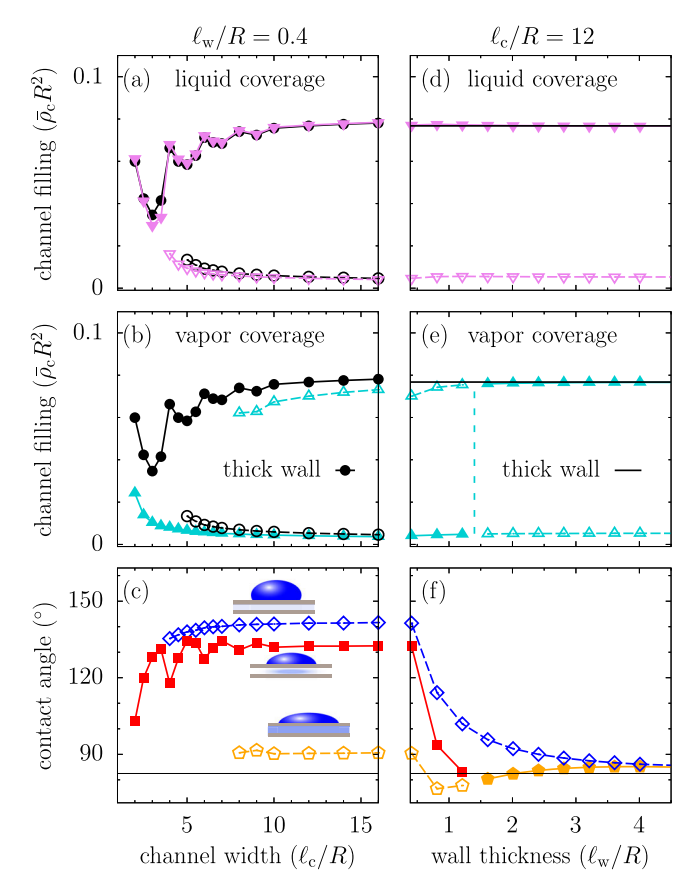


Fig. 3 | Moderately lyophilic walls. Average number densities inside the channel as functions of the channel width for the upper wall covered with a liquid and b vapor, respectively. The thickness of the upper wall is $\ell_w/R = 0.4$, where R is the radius of the fluid particles. The filled symbols and solid lines (open symbols and dashed lines) correspond to stable (metastable) configurations. The black symbols and lines show the case of a thick wall. c Contact angle θ for various configurations illustrated by the droplet cartoons (for visualization purposes only). The contact angles were computed from the surface tensions of the corresponding configurations according to Eq. (1). The blue diamonds and orange pentagons correspond to channels filled with vapor and liquid, respectively, as in Fig. 2. The red squares correspond to a configuration with the channel filled with vapor, with the exception of the region underneath the droplet, which stabilizes the capillary liquid phase. The filled (open) symbols show the stable (metastable) configurations. The horizontal line indicates the reference contact angle $\theta_{\rm ref}$ \approx 82° (no channel; see the dashed green vertical line in Fig. 1b). Results for $\ell_w/R = 2$ are shown in Supplementary Fig. S4. **d**-**f** The same as (a-c) but plotted as functions of ℓ_w/R for channel width $\ell_c/R = 12$. The vertical dashed line in (e) indicates the location of the capillary liquid-vapor transition. Such a transition is absent for the liquid coverage shown in (d).

fluid-fluid interactions, coupled via the reduced liquid density within the channel (Fig. 3b).

In addition to these two metastable configurations, a third configuration arises in which a sessile droplet stabilizes a pancake-like capillary liquid underneath it, which, in turn, is surrounded by the capillary vapor, essentially forming a liquid-vapor interface within the channel (solid red squares in Fig. 3c). The stability of this arrangement for macroscopically large droplets follows the stability of capillary liquid and vapor as obtained for liquid and vapor coverages, respectively (Fig. 3a, b). The associated contact angle falls between the contact angles induced by channels filled with liquid and vapor.

Figure 3d–f show that the behavior described above persists also for thicker walls. However, for $\ell_{\rm w} \gtrsim 1.5R$, the capillary liquid phase becomes stable even for vapor coverage, which renders the capillary vapor phase metastable (Fig. 3e). This behavior implies that the configuration featuring a capillary liquid-vapor interface within the channel becomes unstable as the capillary liquid phase beneath the droplet would expand *ad infinitum* in

order to minimize the grand potential, indicating an $\ell_{\rm w}$ -induced transition in the channel filling.

Discussion

Using classical DFT, we have studied capillary effects in narrow channels, focusing on how wall transparency influences wetting and channel filling. For thick walls, which do not exhibit wall transparency, we revealed a cascade of re-entrant capillary transitions for moderately lyophilic channels characterized by contact angles close to $\theta_{\rm ref} = 90^{\circ}$ (Fig. 1b). The line of first-order capillary phase transitions exhibited a zig-zag behavior, which we attributed to liquid layering within the channel (Fig. 1b).

For a wall sufficiently thin to permit cross-wall interactions between fluid particles, the wetting and channel filling depended sensitively on θ_{ref} . Capillary vapor remained stable for lyophobic walls, regardless of the wall thickness and the kind of fluid coverage; however, both parameters influenced the metastability region of the capillary liquid phase. Interestingly, channels filled with vapor could significantly increase the contact angle of the upper wall, with enhancements up to ca. 30° (Fig. 2d). Remarkably, even for lyophilic solid materials, we obtained highly lyophobic contact angles. For example, vapor filling raised the contact angle to as high as 130°, showing an augmentation of ca. 60° (Fig. 3c, f). This behavior indicates a promising strategy for enhancing surface lyophobicity through vapor-filled porosity. Although our study focused on a generic non-polar van der Waals fluid, we do not expect significant deviations for water. While water molecules experience additional dipole-dipole interactions (decaying as $1/r^3$, where r is the center-to-center distance between two molecules), the thermally averaged dipolar contribution decays as $1/r^6$ —effectively contributing to the van der Waals interactions—and thus is captured by our modeling. Short-ranged hydrogen bonding is unlikely to affect the observed phenomena. Some subtleties might arise if the orientational degrees of freedom of water molecules are constrained near the walls, necessitating a more detailed treatment, which explicitly includes dipolar interactions. Nevertheless, since such interactions are even more long-ranged than simple van der Waals forces, we expect them to amplify the effects reported here. Thus, our finding that vapor-filled porosity can significantly enhance surface lyophobicity suggests practical pathways for designing superhydrophobic surfaces. Transparent walls could also help to mitigate the collapse of the superhydrophobic Cassie-Baxter state⁴⁰ and potentially reduce contact angle hysteresis⁴¹ by minimizing interfacial pinning.

We observed a particularly intriguing wetting behavior for moderately lyophilic transparent walls. Specifically, vapor coverage could stabilize capillary vapor within a channel that would otherwise exhibit capillary condensation (Fig. 3b). This finding holds significant implications for material science, particularly in determining the pore-size distribution (PSD) of porous materials, which commonly relies on classical DFT calculations of $\rm CO_2/N_2$ adsorption isotherms⁴². Current methodologies for PSD computations neglect the effects of wall transparency. We expect that our study will inspire detailed investigations in this research area, potentially prompting the reassessment of these widely used methods for porous materials containing thin walls.

The stabilization of capillary phases through wall coverage could lead to unusual configurations, such as a droplet on the upper wall inducing a pancake-like capillary liquid, surrounded by a capillary vapor phase (Fig. 3c). Thus, a sessile droplet on a thin wall can enforce an inhomogeneous density profile within the channel, characterized by a capillary liquid – capillary vapor interface. This kind of behavior can be exploited for creating heterogeneous patterns inside a channel by arranging liquid droplets on its upper thin wall. This approach can open avenues for investigating complex capillary phenomena, such as two-step condensation⁴³ and three-phase coexistence⁴⁴, paving the way for innovative studies in capillarity and interfacial science.

Future work can extend the phenomena revealed here to canonical ensembles, away from bulk coexistence, and channels made of different wall materials, offering additional means to control channel filling, interfacial properties, and wetting behavior. Even richer scenarios may emerge in ionic

fluids, where (unscreened) electrostatic interactions decay as 1/*r*—far more slowly than van der Waals forces. Although conductive walls can (at least partially) screen such long-ranged cross-wall interactions, they can also induce striking effects such as wall-mediated like-charge attraction⁴⁵, with potential implications for areas like energy storage and nanoscale electrochemistry. Moreover, investigating how wall transparency influences interface localization-delocalization transitions^{39,46,47} could advance our understanding of interfacial stability and phase behavior. We expect such studies to deepen our understanding of confined fluids and interfacial phenomena. Moreover, they may inspire innovative strategies for designing advanced materials at the nanoscale.

Methods

In order to compute the corresponding surface tensions, we employed classical DFT. Within DFT, the fluid number density ρ as a function of position r is obtained by solving a non-linear integral equation

$$\rho(\mathbf{r}) = \Lambda^{-3} \exp\left\{\beta\mu - \beta\Phi_{\rm ext}(\mathbf{r}) + \frac{\delta F_{\rm ex}[\rho]}{\delta\rho}\right\},\tag{3}$$

where Λ is the de Broglie wavelength, μ is the chemical potential, $\Phi_{\rm ext}$ is the external (wall) potential, and $F_{\rm ex}$ is the density-dependent excess free energy functional. We considered $F_{\rm ex}$ to consist of two contributions: (1) hard-core interactions, modeled using fundamental measure theory 32 (FMT), which is known to describe these interactions remarkably well 33,34 ; (2) Lennard-Jones (LJ) interactions between fluid particles and between fluid and solid particles, described within mean-field theory (MFT).

In all calculations, we set the Lennard-Jones interaction cutoff to $R_{\rm cut}=8R$. Increasing $R_{\rm cut}$ would amplify the interactions through the wall, enhancing the effects discussed below. We set the temperature at $T\approx 0.71T_{\odot}$ where $T_{\rm c}$ is the critical temperature ($\epsilon_{\rm ff}/k_{\rm B}T_{\rm c}\approx 0.704$, where $\epsilon_{\rm ff}$ is the Lennard-Jones interaction parameter for fluid particles), and the chemical potential to $\beta\mu=-4.793$, which corresponds to bulk liquid-vapor coexistence. We numerically solved Eq. (3) using the Picard iteration method⁴⁸. Numerical details are presented in Supplementary Notes 1 and 2.

Data availability

The data that support the findings of this study are available from the corresponding author upon reasonable request.

Code availability

The code used to obtain the findings of this study is available from the corresponding author upon reasonable request.

Received: 5 March 2025; Accepted: 23 July 2025; Published online: 13 August 2025

References

- de Gennes, P.-G., Brochard-Wyart, F. & Quéré, D. Capillarity and Wetting Phenomena (Springer, 2004).
- Meinzer, F. C., Clearwater, M. J. & Goldstein, G. Water transport in trees: current perspectives, new insights and some controversies. *Environ. Exp. Bot.* 45, 239–262 (2001).
- Kerstiens, G. Water transport in plant cuticles: an update. J. Exp. Bot. 57, 2493–2499 (2006).
- Stewart, T. D. Tribology of artificial joints. Orthop. Trauma 24, 435–440 (2010).
- Meng, Y., Xu, J., Jin, Z., Prakash, B. & Hu, Y. A review of recent advances in tribology. *Friction* 8, 221–300 (2020).
- Checco, A. et al. Collapse and reversibility of the superhydrophobic state on nanotextured surfaces. *Phys. Rev. Lett.* 112, 216101 (2014).
- Jeevahan, J., Chandrasekaran, M., Britto Joseph, G., Durairaj, R. B. & Mageshwaran, G. Superhydrophobic surfaces: a review on fundamentals, applications, and challenges. *J. Coat. Technol. Res.* 15, 231–250 (2018).

- Parvate, S., Dixit, P. & Chattopadhyay, S. Superhydrophobic surfaces: insights from theory and experiment. *J. Phys. Chem. B* 124, 1323–1360 (2020).
- Convery, N. & Gadegaard, N. 30 years of microfluidics. *Micro Nano Eng.* 2, 76–91 (2019).
- Bonn, D., Eggers, J., Indekeu, J., Meunier, J. & Rolley, E. Wetting and spreading. Rev. Mod. Phys. 81, 739–805 (2009).
- Kaplan, W. D., Chatain, D., Wynblatt, P. & Carter, W. C. A review of wetting versus adsorption, complexions, and related phenomena: the rosetta stone of wetting. *J. Mater. Sci.* 48, 5681–5717 (2013).
- 12. Hauer, L. et al. Wetting on Silicone Surfaces. Soft matter 20, 5273–5295 (2024).
- Furukawa, H., Cordova, K. E., O'Keeffe, M. & Yaghi, O. M. The chemistry and applications of metal-organic frameworks. *Science* 341, 1230444 (2013).
- Wang, C., Liu, X., Keser Demir, N., Chen, J. P. & Li, K. Applications of water stable metal-organic frameworks. *Chem. Soc. Rev.* 45, 5107–5134 (2016).
- Simon, P. & Gogotsi, Y. Materials for electrochemical capacitors. *Nat. Mater.* 7, 845–854 (2008).
- González, A., Goikolea, E., Barrena, J. A. & Mysyk, R. Review on supercapacitors: technologies and materials. *Renew. Sust. Energ. Rev.* 58, 1189–1206 (2016).
- Novoselov, K. S. et al. Electric field effect in atomically thin carbon films. Science 306, 666–669 (2004).
- lijima, S. Helical microtubules of graphitic carbon. *Nature* 354, 56–58 (1991).
- Naguib, M., Mochalin, V. N., Barsoum, M. W. & Gogotsi, Y. 25th anniversary article: MXenes: a new family of two-dimensional materials. Adv. Mater. 26, 992–1005 (2014).
- Mendez-Morales, T., Burbano, M., Haefele, M., Rotenberg, B. & Salanne, M. Ion-Ion correlations across and between electrified graphene layers. J. Chem. Phys. 148, 193812 (2018).
- Kondrat, S., Vasilyev, O. A. & Kornyshev, A. A. Feeling your neighbors across the walls: how interpore ionic interactions affect capacitive energy storage. J. Phys. Chem. Lett. 10, 4523–4527 (2019).
- Rafiee, J. et al. Wetting transparency of graphene. Nat. Mater. 11, 217–222 (2012).
- Chae, S. et al. Lattice transparency of graphene. Nano Lett. 17, 1711–1718 (2017).
- Liu, R., Liu, Z., Zhao, Y., Cui, P. & Wu, H. Role of carbon nanotube wetting transparency in rapid water transport for a nanopore membrane. *Nano Lett.* 24, 3484–3489 (2024).
- Coquinot, B. et al. Momentum tunnelling between nanoscale liquid flows. Nat. Nanotechnol. 20, 397–403 (2025).
- Jeong, D. W. et al. Electron-transfer transparency of graphene: fast reduction of metal ions on graphene-covered donor surfaces. *Phys.* Status Solidi Rapid Res. Lett. 9, 180–186 (2015).
- Evans, R. The nature of the liquid-vapour interface and other topics in the statistical mechanics of non-uniform, classical fluids. *Adv. Phys.* 28, 143–200 (1979).
- 28. Jeanmairet, G., Levy, N., Levesque, M. & Borgis, D. Introduction to classical density functional theory by a computational experiment. *J. Chem. Educ.* **91**, 2112–2115 (2014).
- te Vrugt, M., Löwen, H. & Wittkowski, R. Classical dynamical density functional theory: from fundamentals to applications. *Adv. Phys.* 69, 121–247 (2020).
- Aarts, D. G. A. L., Schmidt, M. & Lekkerkerker, H. N. W. Direct visual observation of thermal capillary waves. *Science* 304, 847–850 (2004).
- 31. Hofmann, T. et al. Wetting of nanopatterned grooved surfaces. *Phys. Rev. Lett.* **104**, 106102 (2010).
- Rosenfeld, Y. Free-energy model for the inhomogeneous hard-sphere fluid mixture and density-functional theory of freezing. *Phys. Rev. Lett.* 63, 980–983 (1989).

- Roth, R., Evans, R., Lang, A. & Kahl, G. Fundamental measure theory for hard-sphere mixtures revisited: the white bear version. *J. Phys. Condens. Matter* 14, 12063 (2002).
- Hansen-Goos, H. & Roth, R. Density functional theory for hard-sphere mixtures: the white bear version mark II. J. Phys. Condens. Matter 18, 8413 (2006).
- Tschopp, S. M., Vuijk, H. D., Sharma, A. & Brader, J. M. Mean-field theory of inhomogeneous fluids. *Phys. Rev. E* 102, 042140 (2020).
- Simon, A. & Oettel, M. Machine learning approaches to classical density functional theory preprint at: https://doi.org/10.48550/arXiv. 2406.07345 (2024).
- Evans, R., Marconi, U. M. B. & Tarazona, P. Fluids in narrow pores: adsorption, capillary condensation, and critical points. *J. Chem. Phys.* 84, 2376–2399 (1986).
- Evans, R. Fluids adsorbed in narrow pores: phase equilibria and structure. J. Phys. Condens. Matter 2, 8989 (1990).
- Parry, A. O. & Evans, R. Influence of wetting on phase equilibria: a novel mechanism for critical-point shifts in films. *Phys. Rev. Lett.* 64, 439–442 (1990).
- 40. Giacomello, A., Schimmele, L., Dietrich, S. & Tasinkevych, M. Perpetual superhydrophobicity. *Soft Matter* **12**, 8927–8934 (2016).
- Giacomello, A., Schimmele, L. & Dietrich, S. Wetting hysteresis induced by nanodefects. *Proc. Natl. Acad. Sci. USA* 113, E262–E271 (2016).
- Landers, J., Gor, G. Y. & Neimark, A. V. Density functional theory methods for characterization of porous materials. *Colloids Surf. A Physicochem. Eng. Asp.* 437, 3–32 (2013).
- Láska, M., Parry, A. O. & Malijevský, A. Breaking Cassie's Law for condensation in a nanopatterned slit. *Phys. Rev. Lett.* 126, 125701 (2021).
- Láska, M., Parry, A. O. & Malijevský, A. Three-phase fluid coexistence in heterogenous slits. *Phys. Rev. Lett.* 124, 115701 (2020).
- Juarez, F. et al. Defying Coulomb's law: a lattice-induced attraction between lithium ions. Carbon 139, 808–812 (2018).
- Milchev, A., Müller, M., Binder, K. & Landau, D. P. Interface localization-delocalization in a double wedge: a new universality class with strong fluctuations and anisotropic scaling. *Phys. Rev. Lett.* 90, 136101 (2003).
- Kondrat, S., Vasilyev, O. A. & Dietrich, S. Probing interface localization-delocalization transitions by colloids. *J. Phys. Condens. Matter* 30, 414002 (2018).
- Mairhofer, J. & Gross, J. Numerical aspects of classical density functional theory for one-dimensional vapor-liquid interfaces. *Fluid Phase Equilib.* 444, 1–12 (2017).

Author contributions

S.K., L.S., A.G., M.T., and S.D. conceived and designed the study. L.S. developed the numerical code. S.K. performed the calculations and

analyzed the data together with L.S. and M.T. S.K. wrote the main manuscript, and M.T. prepared the supplementary materials. All authors contributed to analysing the results, revising the manuscript, and addressing the reviewers' comments.

Funding

Open Access funding enabled and organized by Projekt DEAL.

Competing interests

The authors declare no competing interests.

Additional information

Supplementary information The online version contains supplementary material available at https://doi.org/10.1038/s42005-025-02239-2.

Correspondence and requests for materials should be addressed to Svyatoslav Kondrat.

Peer review information Communications Physics thanks Nikita Kavokine and the other, anonymous, reviewer(s) for their contribution to the peer review of this work. A peer review file is available.

Reprints and permissions information is available at http://www.nature.com/reprints

Publisher's note Springer Nature remains neutral with regard to jurisdictional claims in published maps and institutional affiliations.

Open Access This article is licensed under a Creative Commons Attribution 4.0 International License, which permits use, sharing, adaptation, distribution and reproduction in any medium or format, as long as you give appropriate credit to the original author(s) and the source, provide a link to the Creative Commons licence, and indicate if changes were made. The images or other third party material in this article are included in the article's Creative Commons licence, unless indicated otherwise in a credit line to the material. If material is not included in the article's Creative Commons licence and your intended use is not permitted by statutory regulation or exceeds the permitted use, you will need to obtain permission directly from the copyright holder. To view a copy of this licence, visit https://creativecommons.org/licenses/by/4.0/.

© The Author(s) 2025